Journal of Alloys and Compounds 512 (2012) 115–120

Contents lists available at SciVerse ScienceDirect

Journal of Alloys and Compounds

journal homepage: www.elsevier.com/locate/jallcom

Annealing temperature dependence of the optical and structural properties of selenium-rich CdSe thin films

H. Mahfoz Kotb*, M.A. Dabban, A.Y. Abdel-latif, M.M. Hafiz

Physics Department, Faculty of Science, Assiut University, Assiut 71516, Egypt

ARTICLE INFO

Article history:
Received 6 June 2011
Received in revised form
10 September 2011
Accepted 13 September 2011
Available online 29 September 2011

Keywords:
Optical properties
CdSe thin films
Dispersion parameters
Annealing effect

ABSTRACT

Structural and optical properties of selenium-rich CdSe (SR-CdSe) thin films prepared by thermal evaporation are studied as a function of annealing temperature. X-ray diffraction (XRD) patterns show that the as-prepared films were amorphous, whereas the annealed films are polycrystalline. Analyzing XRD patterns of the annealed films reveal the coexistence of both (hexagonal) Se and (hexagonal) CdSe crystalline phases. Surface roughness of SR-CdSe films is measured using atomic force microscope (AFM). Analyses of the absorption spectra in the wavelength range (200–2500 nm) of SR-CdSe thin films indicates the existence of direct and indirect optical transition mechanisms. The optical band gap (E_g) of as-prepared film is 1.92 and 2.14 eV for the indirect allowed and direct allowed transitions respectively. After annealing, the absorption coefficient and optical band gap were found to decrease, while the values of refractive index (n) and the extinction coefficient (k_{ex}) increase. The dispersion of the refractive index is described using the Wimple–Di Domenico (WDD) single oscillator model and the dispersion parameters are calculated as a function of annealing temperature. Besides, the high frequency dielectric constant (ε_∞) and the ratios of the free carrier concentration to its effective mass (N/m^*) are studied as a function of annealing temperature. The results are discussed and correlated in terms of amorphous-crystalline transformations.

1. Introduction

Chalcogenide glasses have many interesting properties and applications [1,2]. Cadmium selenide system is an example of the wide-bandgap II–VI systems that is considered as a promising semiconductor material for optoelectronics and photovoltaic devices [3–5]. Thin films of CdSe have been deposited using different techniques such as electron beam deposition [6], spray pyrolysis [7], vacuum deposition [8] and chemical bath deposition [9]. Electrical and optical properties of these semiconducting films are found to be sensitive to ambient conditions and deposition technique. The thin film growth conditions and thermal annealing process were found effective to achieve the performance devices [10–12]. The stoichiometry of the films is expected also to have a significant influence on the electrical and optical properties of these films. However; no enough studies are reported on the growth, characterization and properties of non-stoichiometric films [13]. Previously we have studied the electrical properties of selenium-rich cadmium selenide, SR-CdSe, thin films deposited by thermal evaporation [14]. The aim of the present work is to study the influence of thermal annealing on the structural, spectral behavior and optical constants of thermally evaporated SR-CdSe, $Cd_{10}Se_{90}$, thin films.

2. Experimental techniques

The bulk $Cd_{10}Se_{90}$ were prepared from a mixture of Cd and Se elements with purity 99.999% (Aldrich Chem Co., USA). The constituent elements were weighed according to their atomic percentage and were sealed in a quartz ampoule (inner diameter ~ 8 mm) under vacuum of 10^{-3} T. The sealed ampoules were kept inside a furnace and heated gradually up to 1173 K and kept at that temperature for 16 h. Continuous stirring of the melt was carried out to ensure good homogeneity. The melt was then rapidly quenched in ice–water mixture. After quenching, the solid ingots were removed from the ampoules and kept in dry atmosphere.

Thin films of SR-CdSe were then deposited onto well-cleaned glass substrates kept at room temperature by thermal evaporation technique using a high vacuum coating unit (E306A, Edwards Co., UK). During the deposition process (at normal incidence), the substrates were suitably rotated in order to obtain films of uniform thickness. The thickness of the films (~150 nm and 600 nm for optical and structural respectively) was measured by a mechanical profilometer (KLA Tenchor P.15). Annealing of the films was carried out in Pyrex tube furnace at 348 K, 373 K, 398 K and 423 K for 30 min under flow of pure nitrogen in order to avoid the oxidation of the samples during annealing.

The structure and phases of the films were confirmed by using X-ray diffractometer (Philips type PW 1710 with Cu as a target and Ni as a filter, $\lambda = 1.5418$ Å). The surface roughness of the films was measured using the Digital Instrument 3100 Atomic Force Microscope (AFM). The chemical composition of the films was studied using the standard energy dispersive analysis of X-ray (EDX) technique. An EDX unit

* Corresponding author. Tel.: +20 10 8771059; fax: +20 88 2354130.
E-mail address: hmkscience@yahoo.com (H.M. Kotb).

0925-8388/$ – see front matter © 2011 Elsevier B.V. All rights reserved.
doi:10.1016/j.jallcom.2011.09.034

attached to the scanning electron microscope (SEM), Jeol (JSM)-T200 type, was used for these measurements.

The optical transmittance, *T*, and reflectance, *R*, of the films were measured at room temperature with unpolarized light at normal incidence in the wavelength range (200–2500 nm) using a double beam (ultraviolet–visible) scanning spectrophotometer (SHIMADZU 2101) attached to a personal computer.

3. Results and discussions

3.1. Structural analysis: EDX, XRD, SEM and AFM

The EDX analysis of as-prepared thin film yielded an average atomic percentage of Cd:Se of 9.92:90.08 which is very near to our targeted Cd:Se ratio (10:90). X-ray diffraction patterns of as-prepared and annealed films are shown in Fig. 1. As-prepared films were of amorphous nature, Fig. 1(a). However, thin films annealed for 30 min in N_2 atmosphere at 348 K, 373 K and 423 K, Fig. 1(b)–(d) shows a polycrystalline structure indicating an amorphous-to-crystalline phase transition. Peaks were indexed according to JCPDS files no. 02-0330 and no. 86-2246 for hexagonal CdSe and hexagonal Se respectively.

The annealed films at 348 K and 373 K, Fig. 1(b) and (c), are characterized by the predominant appearance of Se hexagonal phase peaks. Only one tiny peak situated at $2\theta = 25.18^\circ$ ($d = 3.537$ Å) is corresponding to (0 0 2) plane of CdSe hexagonal phase. With further increase of the annealing temperature up to 423 K, the CdSe peak showed a much greater intensity which indicates a considerable increase in the volume fraction of CdSe crystalline phase.

The interplanar spacing (d) was calculated using Bragg's formula ($d = \lambda/2 \sin\theta$) where θ is the Bragg's angle, λ is the wavelength of the used X-ray. The lattice constant (c) for different SR-CdSe films was calculated for hexagonal structure by the equation [15]:

$$\frac{1}{d_{hkl}^2} = \frac{4}{3}\left[\frac{h^2 + hk + k^2}{a^2}\right] + \frac{l^2}{c^2} \quad (1)$$

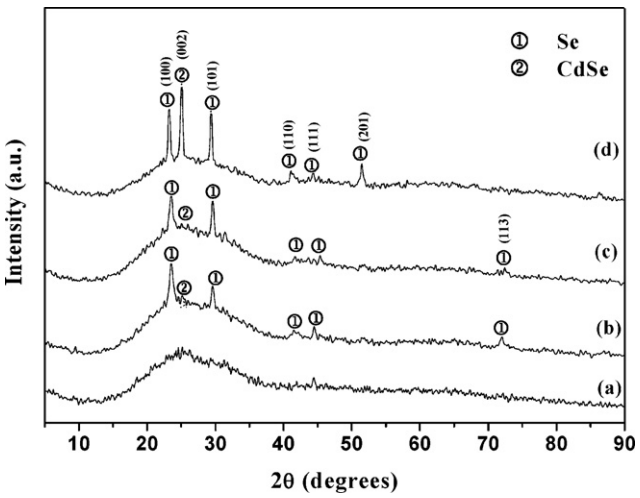

Fig. 1. XRD patterns of $Cd_{10}Se_{90}$ thin films: (a) as-prepared, (b) annealed at 348 K, (c) annealed at 373 K, (d) annealed at 423 K.

From Table 1, we note that the calculated values for the parameters d and c for SR-CdSe thin films are in a good agreement with the standard JCPDS data files for Se and CdSe hexagonal phases. In fact the tensile strain of the annealed films of SR-CdSe [14] is thought to be the reason of the relatively larger values of these parameters for SR-CdSe as compared to the standard lattice parameters.

Fig. 2 shows the AFM images of the as-prepared SR-CdSe film and after annealing at 423 K. Before annealing the root mean square (RMS) roughness was 3.31 nm. After annealing, the RMS roughness of the surface decreased to 1.45 nm. This may be understood as some small amounts of material diffuse from the surface to the inside of the film during the annealing process resulting in a roughness reduction and grain growth.

Table 1
Structure parameters of annealed SR-CdSe thin films.

Phase	Annealing temperature (K)	*h k l*	Lattice spacing, *d* (Å)		Lattice parameters, *c* (Å)	
			Observed	Standard	Observed	Standard
CdSe	348	0 0 2	3.537	3.52	7.074	7.02
	373	0 0 2	3.553		7.106	
	423	0 0 2	3.553		7.106	
Se	348	1 0 1	3.017	3.007	5.006	4.958
	373	1 0 1	3.073		4.989	
	423	1 0 1	3.072		4.998	

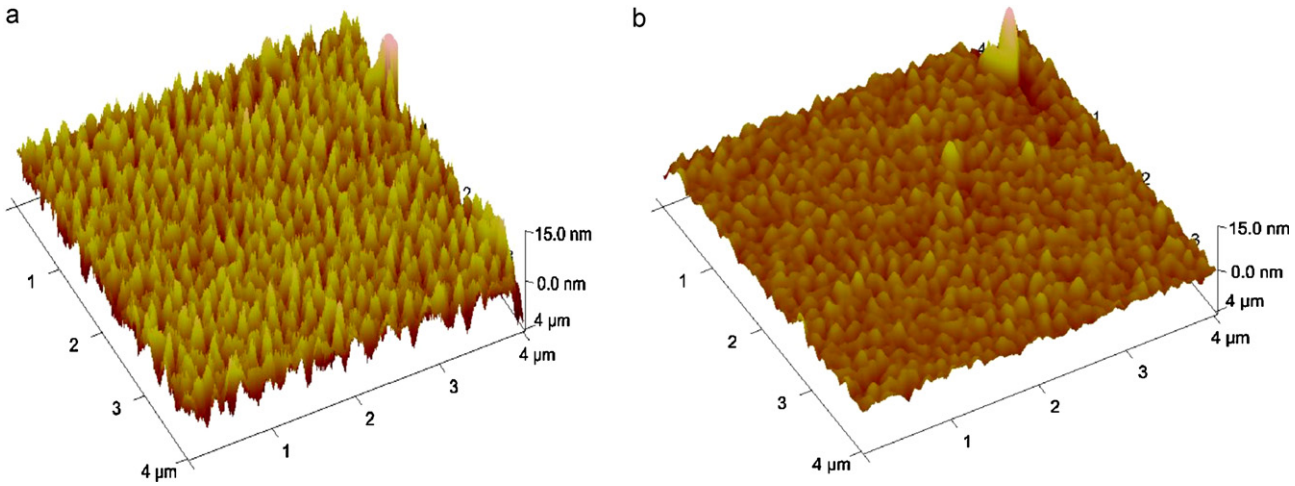

Fig. 2. AFM image for SR-CdSe thin film: (a) before and (b) after annealing at 423 K for 30 min.

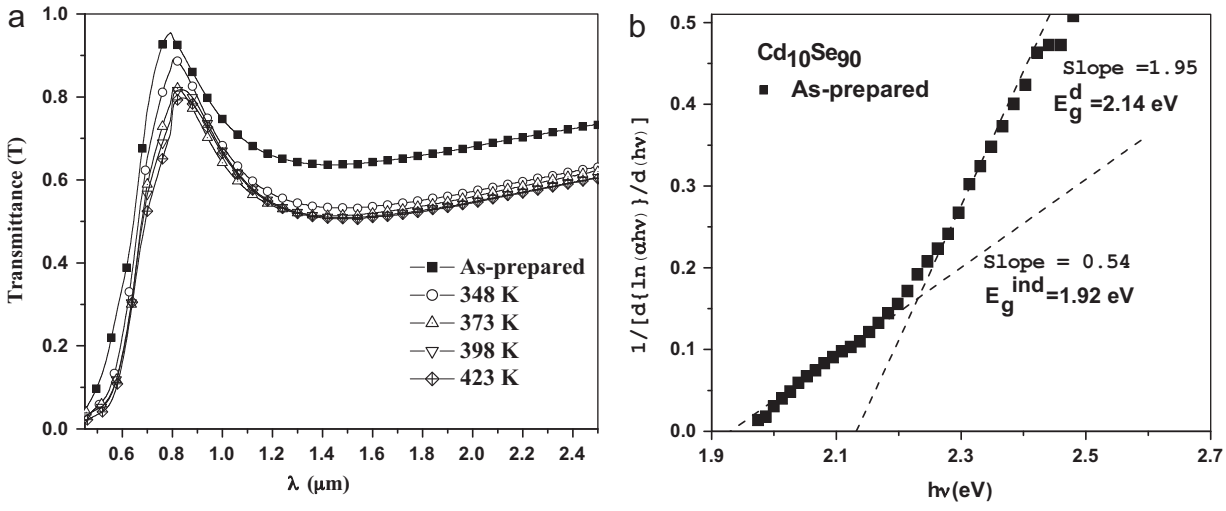

Fig. 3. (a) The spectral distribution of the optical transmittance for as-prepared and annealed SR-CdSe thin films. (b) Example for the plot of $1/[d\{\ln(\alpha h\nu)\}/d(h\nu)]$ versus $h\nu$ for as-prepared.

3.2. Optical properties

3.2.1. The optical constants

The optical constants were deduced from the transmittance (T) and reflectance (R) data. Fig. 3(a) shows the transmittance, T, versus wavelength, λ, for as-prepared and annealed SR-CdSe thin films in the spectral range 450–2500 nm. As can be seen in Fig. 3(a), the changes in the optical transmission of annealed SR-CdSe films show the shifts of the high energy absorption edges to higher wavelengths with increasing the annealing temperature (348–423 K).

Using the measured data of the transmittance (T) and reflectance (R), the absorption coefficient α have been computed by using [16],

$$\alpha = \frac{1}{d}\ln\left[\frac{(1-R)^2}{2T} + \left\{\left(\frac{(1-R)^2}{2T}\right)^2 - R^2\right\}^{1/2}\right] \quad (2)$$

where d is the films thickness.

In the high absorption region ($\alpha \geq 10^4\ \mathrm{cm}^{-1}$), the variation of the absorption coefficient with photon energy is obtained as [17]:

$$\alpha h\nu = B(h\nu - E_g)^r \quad (3)$$

where h is Planck constant, ν is the frequency, B is an energy-independent constant (it is a parameter which depends on the transition probability), E_g is the optical energy gap of the investigated films, and r is a number characterizing the transition process, having the values (1/2, 3/2, 2 and 3) for direct allowed, direct forbidden, indirect allowed and indirect forbidden transitions, respectively.

By simple mathematical treatment, Eq. (3) can be written as,

$$\frac{1}{[d\left\{\ln(\alpha h\nu)\right\}/d(h\nu)]} = \frac{1}{r}h\nu - \frac{E_g}{r} \quad (4)$$

Eq. (4) then can be used to deduce the type of transition and the optical energy gap, E_g, for the studied films by plotting $1/[d\{\ln(\alpha h\nu)\}/d(h\nu)]$ versus $h\nu$. Fig. 3(b) represents an example of such a plot for the as-prepared SR-CdSe film. The values of 'r' and 'E_g' can be directly determined from the slope and the intercept of the straight line, respectively. For all SR-CdSe thin films, there were two distinct linear parts of different slopes indicating the existence of both indirect and direct optical transitions ($1/r \approx 0.5 \pm 0.04$ or $\approx 2 \pm 0.05$) for SR-CdSe thin films which is in agreement with the results reported by Patel et al. [18] for thermally evaporated CdSe thin films.

Plots of $(\alpha h\nu)^{1/2}$ and $(\alpha h\nu)^2$ versus $h\nu$, Fig. 4, were used to determine the values E_g^{ind} and E_g^d, for the as-prepared and annealed films respectively. As shown, $(\alpha h\nu)^{1/2}$ and $(\alpha h\nu)^2$ vary linearly with $h\nu$, which is in a good agreement with the classical theory of the band to band transition. Extrapolating the straight parts of the two relations

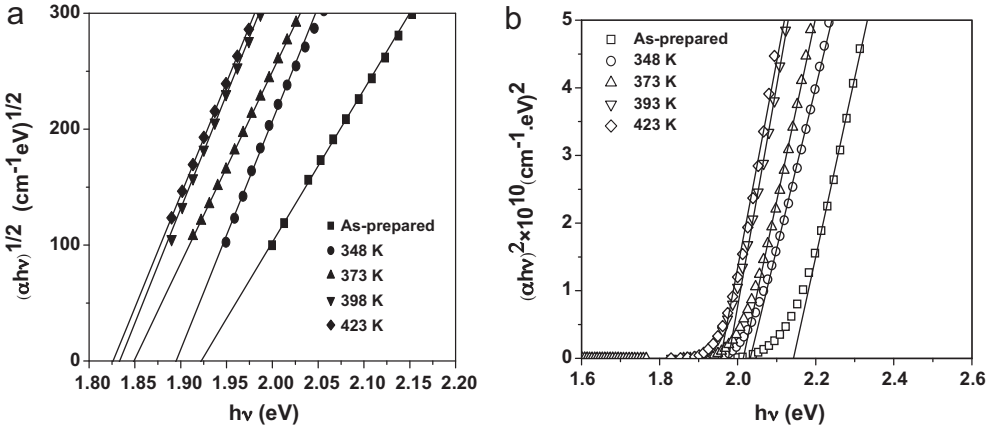

Fig. 4. (a) Plot of $(\alpha h\nu)^{1/2}$ versus $h\nu$ for as-prepared and annealed SR-CdSe thin films. (b) Plot $(\alpha h\nu)^2$ versus $h\nu$ for as-prepared and annealed SR-CdSe thin films.

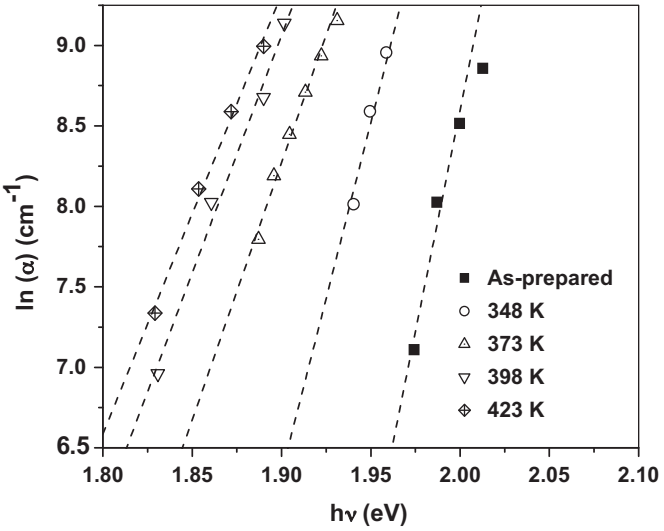

Fig. 5. Plots of ln(α) versus photon energy ($h\nu$) for as-prepared and annealed SR-CdSe thin films.

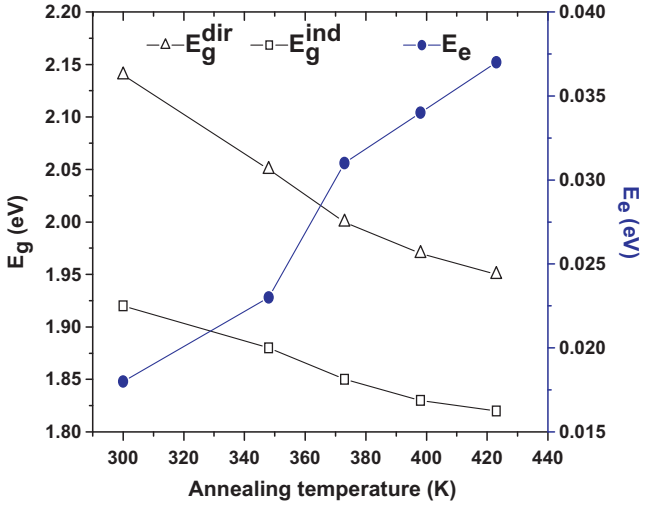

Fig. 6. The values of E_g and E_e as a function of annealing temperature of SR-CdSe thin films.

towards lower photon energies yields the values of the forbidden band gaps.

For absorption coefficient (α) of less than $10^4\,cm^{-1}$, the low absorption region, there is usually Urbach tail where α increases exponentially with the photon energy ($h\nu$) as [19],

$$\alpha(\nu) = \alpha_o \exp\left(\frac{h\nu}{E_e}\right) \quad (5)$$

where ν is the frequency of the radiation, α_o is constant and E_e is often interpreted as the width of the tails of the localized states in the gap region and in general represents the degree of disorder in semiconductors. Thus plotting of ln(α) versus $h\nu$, Fig. 5, should give straight line with the inverse of its slope equals E_e.

The values of the energy gaps, E_g, and the width of localized states tails, E_e, for the as-prepared and annealed SR-CdSe thin films are listed in Table 2 and plotted in Fig. 6. It is clear that the optical energy gap decreases gradually with annealing temperature. This result can be interpreted by assuming the production of surface dangling bonds around the crystallites during the process of crystallization [20]. It has been suggested [21] that 'nearly ideal' amorphous solids crystallize under heat treatment, and that in the process of crystallization dangling bonds are produced around the surface of the crystallites. Further heat treatment causes the crystallites to break down [9] into smaller crystals thereby increasing the number of surface dangling bonds. These dangling bonds are responsible for formation of some types of defects in highly polycrystalline solids. As the number of dangling bonds and defects increases with increase in annealing temperature, the concentration of localized states in the band structure also increases gradually. Hence the heat treatment of the films causes an increase in the energy width of localized states tails thereby reducing the optical band gap. Similar behavior has also been observed for CuGeTe [22] and GeAsTe thin films [23]. The higher values of E_g for SR-CdSe thin films compared to the value of bulk optical gap, E_g, of CdSe (1.74 ± 0.01) eV may be due to the quantum confinement effect accompanying the nanocrystalline nature of SR-CdSe thin films [14]. Similar blue shift in band gap energy values for thin films with the reduction of crystallite sizes have been previously reported for chemically deposited CdSe thin films [24,25].

3.3. Dispersive optical constants

The values of the refractive index (n) were calculated from the reflectance (R) data by the following relation [26],

$$n = \left[\left(\frac{4R}{(R-1)^2} - k_{ex}^2\right)^{1/2} + \frac{(1+R)}{(1-R)}\right] \quad (6)$$

where k_{ex} is the extinction coefficient which is related to the absorption coefficient (α) and the wavelength (λ) by $k_{ex} = \alpha\lambda/4\pi$. The refractive index ($n$) and extinction coefficient (k_{ex}) dependence on the wavelength are shown in Fig. 7. A peak appeared in the refractive index (n) appears at around 600 nm for as-prepared films which shifts to lower energies due to annealing temperatures. Besides, the refractive index values for annealed films are generally higher than its values for as-prepared films.

The dispersion of refractive index (n) may be analyzed using the concept of the single-oscillator and can be expressed by the Wimple–Didomenico relationship [27,28],

$$n^2 = 1 + \frac{E_d E_o}{{E_o}^2 - (h\nu)^2} \quad (7)$$

where E_o is the oscillator energy and considered as an average energy gap, $h\nu$ is the photon energy and E_d is the dispersion energy which measures the average strength of the interband optical transitions.

The dispersion parameters E_d and E_o can be obtained according to Eq. (7) by plotting of $(n^2-1)^{-1}$ versus $(h\nu)^2$ as shown in Fig. 8(a). The values of E_d and E_o can be directly determined from

Table 2
Optical parameters of SR-CdSe thin films.

Ann. temp. (K)	E_e (eV)	E_g^{ind} (eV)	E_g^{dir} (eV)	E_o (eV)	E_d (eV)	$\varepsilon_{\infty(1)}$	N/m^* ($\times 10^{56}\,m^{-3}\,kg^{-1}$)	$\varepsilon_{\infty(2)}$
As	0.018	1.92	2.14	1.92	2.28	13.82	12	2.18
348	0.023	1.88	2.05	1.92	1.26	16.63	13.5	1.63
373	0.031	1.85	2.00	1.94	3.96	18.88	15	3.1
398	0.034	1.83	1.97	1.94	4.74	20.57	17	3.63
423	0.037	1.82	1.95	1.95	5.35	22.93	22	3.7

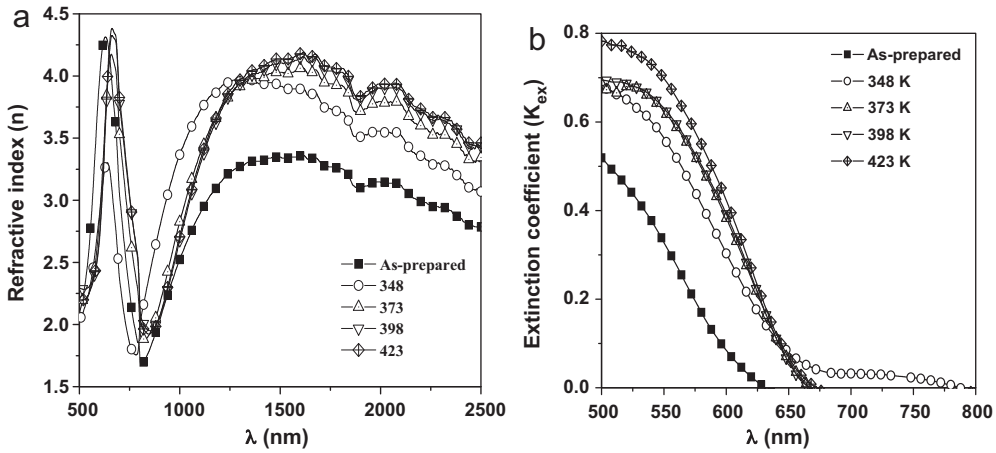

Fig. 7. (a) Dispersion curves of refractive index, n for as-prepared and annealed SR-CdSe thin films. (b) Dispersion curves of extinction coefficient (k_{ex}) for as-prepared and annealed SR-CdSe thin films.

the slope and the intercept with the vertical axis. The obtained values for the dispersion parameters E_o and E_d for the SR-CdSe thin films are given in Table 2. In our case it is found that $E_o \approx E_g$, which is in good agreement with the relation of Tichá and Tichý [29].

3.4. Determination of the high frequency dielectric constants

In order to calculate the high frequency dielectric constant (ε_∞), we have further analyzed the data of refractive index dependence on photon's energy (or wavelength) via two procedures.

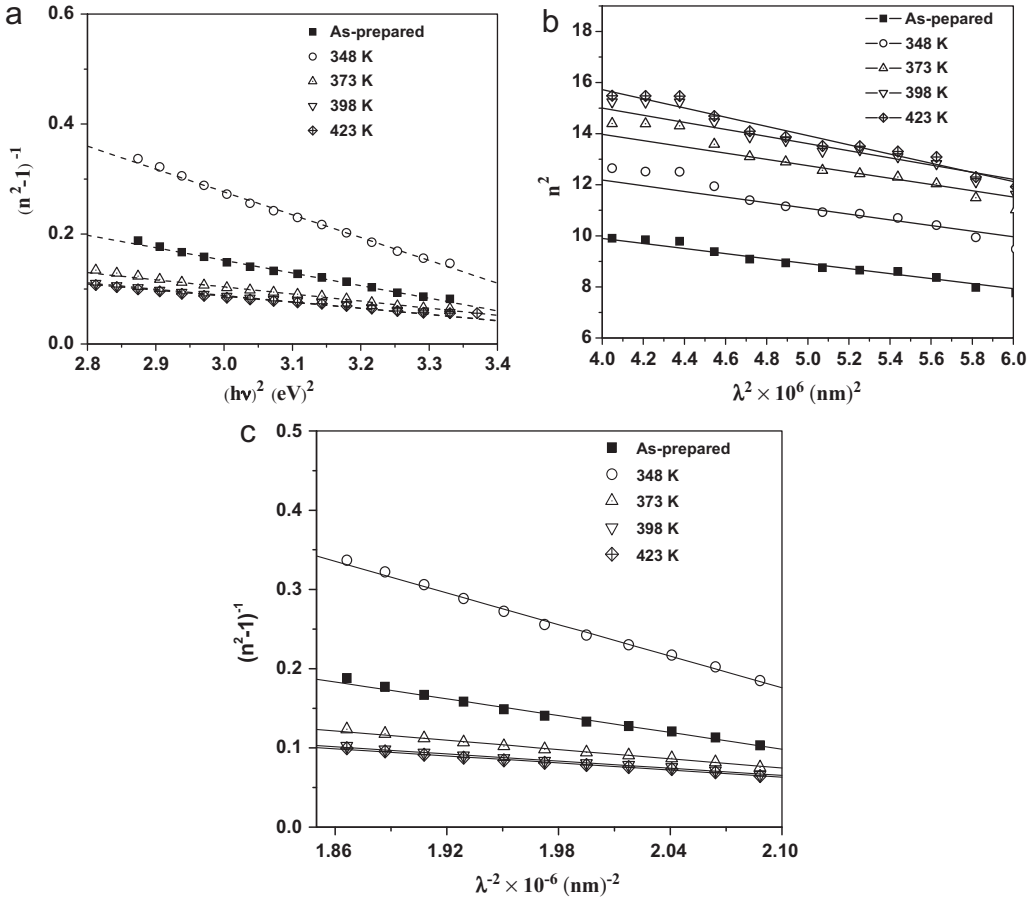

Fig. 8. (a) Plots of $(n^2-1)^{-1}$ versus $(h\nu)^2$ for as-prepared and annealed SR-CdSe thin films. (b) Plots of n^2 versus λ^2 for as-prepared and annealed SR-CdSe thin films. (c) Plots of $1/[1-n^2]$ versus λ^{-2} for as-prepared and annealed SR-CdSe thin films.

The first procedure includes the contribution of free carries and the lattice vibration modes of dispersion. In this procedure, the relation between the lattice high frequency dielectric constant ($\varepsilon_{\infty(1)}$) and refractive index (n) is given by the following relation [30]:

$$n^2 = \varepsilon_{\infty(1)} - \left(\frac{e^2 N}{4\pi c^2 \varepsilon_o m^*}\right)\lambda^2 \quad (8)$$

where e is the electronic charge, ε_o is the vacuum permittivity (8.854×10^{-12} F/m), N is the charge carrier concentration and m^* is the effective mass of the charge carrier. The plot of n^2 versus λ^2 for SR-CdSe thin films is shown in Fig. 8(b). Extrapolating the linear part of this dependence to zero wavelength gives the value of $\varepsilon_{\infty(1)}$ and from the slopes of these lines we can calculate the values of N/m^*. From Table 2, it is clear that the value of $\varepsilon_{\infty(1)}$ increases with increasing the annealing temperature. This behavior can be attributed to the increase in the free carrier concentration (assuming that m^* is constant in the first approximation).

The second procedure for calculating ε_∞ is based upon the dispersion arising from the bound carriers in an empty lattice. In the this procedure, $\varepsilon_{\infty(2)}$ ($= n_\infty^2$) can be calculated by applying the following simple classical dispersion relation using the single term Sellmeir oscillation [31]

$$\frac{({n_\infty}^2 - 1)}{(n^2 - 1)} = 1 - \left(\frac{\lambda_o}{\lambda}\right)^2 \quad (9)$$

where n_∞ is the long wavelength refractive index, λ_o the average oscillator wavelength. Plots of $(n^2 - 1)^{-1}$ versus λ^{-2} for SR-CdSe thin films are given Fig. 8(c). Value of $\varepsilon_{\infty(2)}$ can be calculated according to Eq. (9) and included in Table 2. It is noticed that the values $\varepsilon_{\infty(1)}$ are higher than those of $\varepsilon_{\infty(2)}$. This behavior can be attributed to, the increase in the free carrier contribution [32].

4. Conclusions

Annealing of amorphous SR-CdSe films at temperatures 373–423 K in N_2 atmosphere resulted in polycrystalline films with Se phase in the major proportion as compared to the CdSe phase with both phases exhibit a hexagonal structure. AFM images revealed that the films consisted of homogeneous, uniform grains free from pinholes. Root-mean-square (RMS) roughness of SR-CdSe decreased with annealing.

The optical absorption measurements indicate that the absorption is due to indirect and direct band gap for as-prepared and annealed films. Thermal annealing causes a decrease in optical band gap E_g for SR-CdSe thin films accompanied by an increase of the width of localized states tail, E_e. This behavior is attributed to the production of more surface dangling bonds around the formed crystallites during the process of crystallization. It was found that the dispersion of refractive index obeyed the single oscillator model. The results indicate that the optical parameters E_d, E_o, ε_∞, and N/m^* are sensitive to heat treatment. This confirms the effect of the annealing on the density of localized states and microstructure of the SR-CdSe films.

Acknowledgement

One of the authors, Dr. Hicham M Kotb, wishes to thank deeply the team of LAAS (Toulouse–France) for their support.

References

[1] R.S. Mane, C.D. Lokhande, Mater. Chem. Phys. 65 (2000) 1.
[2] M.M. Hafiz, M.M. Ibrahim, M. Dongol, J. Appl. Phys. 54 (1983) 1950–1954.
[3] A. Reisman, M. Berkenblit, M. Wizen, J. Phys. Chem. 65 (1962) 2210.
[4] A.K. Rautri, R. Thangraj, A.K. Sharama, B.B. Tripathi, O.P. Agnihotri, Thin Solid Films 91 (1982) 55.
[5] D. Haneman, G.H.J. Wanterrar, R.C. Kaainthala, Sol. Energy Mater. 10 (1984) 69.
[6] N.J. Kissinger, M. Jayachandran, K. Permual, S. Raja, Bull. Mater. Sci. 30 (2007) 547.
[7] T. Elango, S. Subermanian, K.R. Maurli, Surf. Coat. Technol. 8 (2003) 123.
[8] K. Sarmah, R. Sarma, H.L. Das, Chalc. Lett. 5 (2008) 153.
[9] S. Erat, H. Metin, M. Ari, Mater. Chem. Phys. 111 (2008) 114.
[10] D. Pathinettam Padiyan, A. Marikani, K.R. Murali, Mater. Chem. Phys. 78 (2002) 51.
[11] S. Velumani, P.J. Xavier Mathew, Sa. Sebastain, K. Narayandass, D. Mangalaraj, Sol. Energy Mater. Sol. Cells 76 (2003) 347.
[12] P.P. Hanker, P.A. Chate, D.J. Sathe, A.A. Patil, J. Mater. Sci. Mater. Electron. 20 (2009) 776.
[13] S.K. Kaushish, T.P. Sharma, Opt. Mater. 14 (2000) 297.
[14] H. Mahfoz Kotb, M.A. Dabban, F.M. Abdel-Rahim, A.Y. Abdel-latif, M.M. Hafiz, Physica B 406 (2011) 1326–1329.
[15] V.K. Pecharsky, Fundamentals of Powder Diffraction and Structural Characterization of Materials, Springer, 2005.
[16] M. El-Nahass, Opt. Laser Technol. 39 (2007) 347–352.
[17] N. Mott, E. Davis, Electronic Process in Non-crystalline Materials, Clarendon Press, Oxford, 1971.
[18] K.D. Patel, M.S. Jani, V.M. Pathak, R. Srivastava, Chalc. Lett. 6 (2009) 279–286.
[19] F. Urbach, Phys. Rev. 92 (1953) 1324.
[20] A. Chaudhuri, S. Chaudhuri, S.K. Biswas, K. Goswami, J. Non-Cryst. Solids 54 (1983) 179.
[21] S. Hasegawa, M. Kitagawa, Solid State Commun. 27 (1978) 855.
[22] H. El-Zahed, Physica B 307 (2001) 95.
[23] S.H. Mohameda, M.M. Wakkad, A.M. Ahmed, A.K. Diab, Eur. Phys. J. Appl. Phys. 34 (2006) 165–171.
[24] C. Mehta, J.M. Abbas, G.S. Saini, S.K. Tripathi, Chalc. Lett. 4 (2007) 133–138.
[25] T.S. Shyju, S. Anandhi, R. Indirajith, R. Gopalakrishnan, J. Alloys Compd. 506 (2010) 892–897.
[26] F. Yakuphanoglu, M. Kandaz, M.N. Yarasır, F.B. S-enkal, Physica B 393 (2007) 235–238.
[27] S.H. Wemple, M. Didomenico, Phys. Rev. B 3 (1971) 1338.
[28] S.H. Wemple, Phys. Rev. B 7 (1973) 3767.
[29] H. Tichá, L. Tichý, J. Optoelectron. Adv. Mater. 4 (2) (2002) 381–386.
[30] J.N. Zemel, J.D. Jensen, R.B. Schoolar, Phys. Rev. A 140 (1965) 330.
[31] A.K. Wolaton, T.S. Moss, Proc. R. Soc. 81 (1963) 5091.
[32] F. Yakuphanoglu, C. Viswanthan, J. Non-Cryst. Solids 353 (2007) 2934–2937.